ELSEVIER

Lithos 55 (2001) 49–68

LITHOS

www.elsevier.nl/locate/lithos

Carbonic inclusions

Alfons Van den Kerkhof [a,*], Régis Thiéry [b]

[a] *IGDL, University of Göttingen, Goldschmidtstrasse 3, 37077 Göttingen, Germany*
[b] *UMR 6524 'Magmas et Volcans', OPGC, Blaise Pascal University 5, rue Kessler, 63038 Clermont-Ferrand, France*

Received 15 September 1999; accepted 4 April 2000

Abstract

The paper gives an overview of the phase relations in carbonic fluid inclusions with pure, binary and ternary mixtures of the system CO_2–CH_4–N_2, compositions, which are frequently found in geological materials. Phase transitions involving liquid, gas and solid phases in the temperature range between −192°C and 31°C are discussed and presented in phase diagrams (*PT*, *TX* and *VX* projections). These diagrams can be applied for the interpretation of microthermometry data in order to determine fluid composition and molar volume (or density).

Keywords: Fluid inclusions; Carbon dioxide; Methane; Nitrogen; Microthermometry

1. Introduction

Gas compositions of non-aqueous fluid inclusions in rocks can be generally represented by the system CO_2–CH_4–N_2. Pure gas compositions (mostly CO_2, sometimes CH_4 or N_2) are commonly found in fluid inclusions, but in many cases, gas mixtures occur. Besides these three gas compounds and water, no other fluid compounds in the system C–O–H–N are normally stable in rocks at room temperature, or they occur in very low concentrations. However, at high temperatures during metamorphism, compounds like CO may be important (e.g. Huizenga, 2001). CO_2 is the most common carbonic component in high-grade metamorphic rocks (Touret, 1977); considerable amounts of CH_4 may form in rocks which have been chemically re-equilibrated during retrograde conditions: the oxygen fugacity being buffered by the rock minerals is reduced towards lower temperatures and may cause a change of the composition of the fluid, which is in equilibrium with the rock. As a consequence of low oxygen fugacity, methane is a common gas compound in diagenetic and low-grade metamorphic rocks (Mullis, 1979). Nitrogen is an important gas component in many rock types, from early diagenetic towards high-grade metamorphic rocks (Dubessy and Ramboz, 1986) and assumed to form by the breakdown of NH_4^+-containing feldspar and mica during prograde metamorphism. N_2-rich fluid inclusions have been frequently found in paragneissic eclogite (Andersen et al., 1990; Klemd et al., 1992). Carbonic fluids in rocks may be of magmatic origin (Touret, 1992), formed by the decomposition

* Corresponding author.
E-mail address: akerkho@gwdg.de (A. Van den Kerkhof).

0024-4937/01/$ - see front matter
PII: S0024-4937(00)00038-4

of organic matter, by oxidation reactions involving graphite or as a reaction product of decarbonization in calc-silicate rocks. In granulite rocks from Bamble (Norway), isotopic evidence has been found for juvenile CO_2 (Hoefs and Touret, 1975; Van den Kerkhof et al., 1994). During the metamorphic evolution, fluids are normally repeatedly re-equilibrated and may be re-trapped at subsequent stages during uplift. Being controlled by the mineral buffer (in respect of fO_2, fN_2, etc.) fluid compositions normally result in (pseudo)binary gas mixtures of CO_2–CH_4 (reducing) or CO_2–N_2 (oxidizing) (Bakker and Jansen, 1993; Huizenga, 1995, 2001); ternary mixtures of about equal amounts of CO_2, CH_4 and N_2 are rare in natural fluid inclusions (Van den Kerkhof, 1988).

The first step and aim of microthermometry experiments (eventually combined with Raman analysis) is the determination of the fluid molar volume

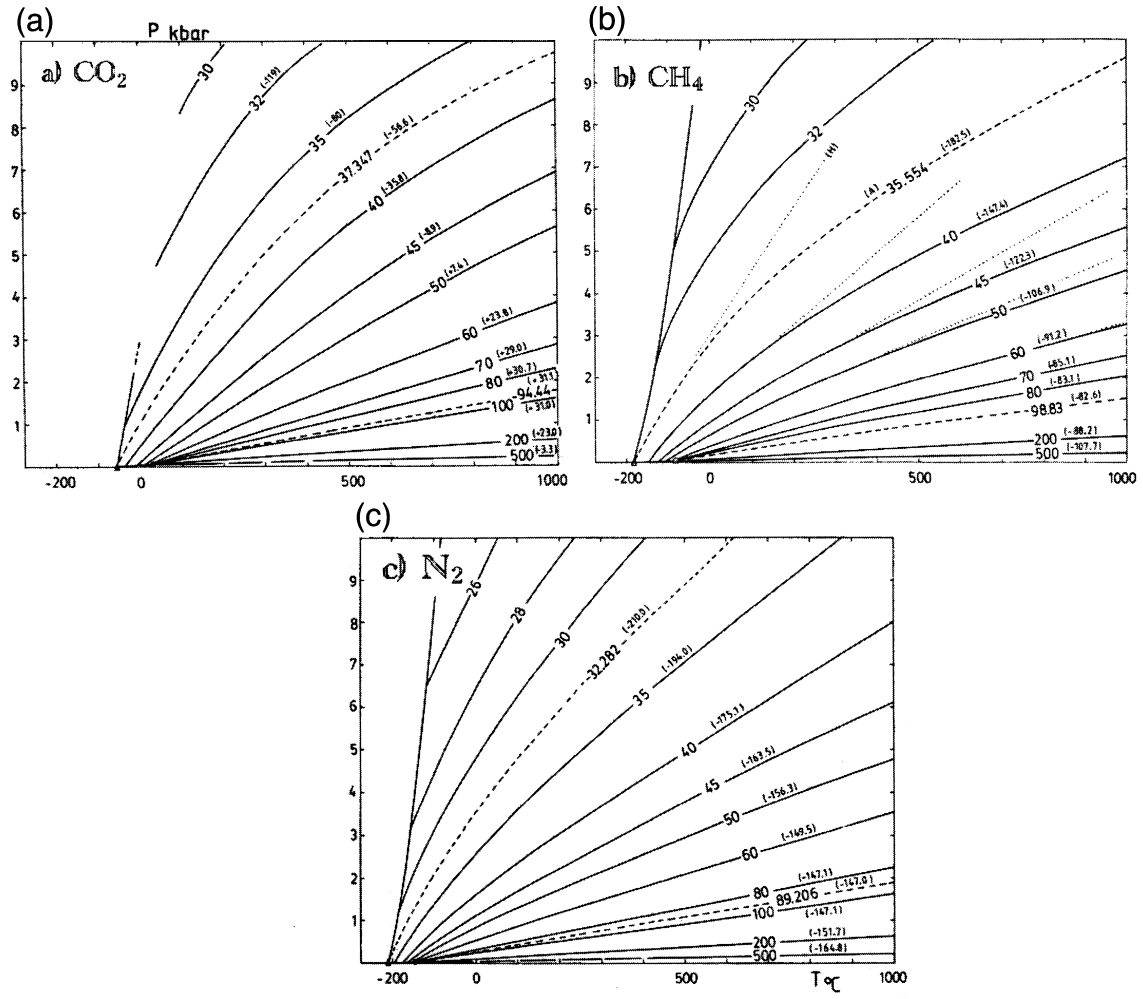

Fig. 1. Isochores for the systems (a) CO_2 (b) CH_4 and (c) N_2 (molar volumes between 30 and 500 cm^3/mole) (after Van den Kerkhof, 1988) compiled from experimental data from the literature: (a) Angus et al. (1976a), Vagarftik (1972), Juza et al. (1965) and Shmonov and Shmulovish (1974); (b) Angus et al. (1976b), Vagarftik (1972), dotted lines are calculated by the equation of state of Holloway (1977); (c) Angus et al. (1979), Vagarftik (1972), Malbrunot and Vodar (1973), Tsiklis and Polyakov (1968) and Antanovish and Plotnikov (1976). Numbers denote molar volumes in cm^3/mole; numbers in brackets are the homogenization temperatures (°C).

(or the density) and the composition, the key parameters to calculate the trapping pressure and temperature (isochore calculation) with the use of an appropriate equation of state (e.g. Holloway, 1977; Kerrick and Jacobs, 1981; Bottinga and Richet, 1981; Brown, 1989). Fig. 1 shows isochores for CO_2, CH_4 and N_2, derived from the literature.

CO_2 with admixtures of other components can be identified by melting temperatures (T_m) markedly lower than -56.6°C, the triple point of CO_2. Methane and nitrogen in carbonic inclusions have considerable effect also on the homogenization temperature (T_h). Burruss (1981) introduced the so-called *VX* diagram, showing the variation of the molar volume (V) with the composition (X) for a given temperature, to demonstrate these effects for the system CO_2–CH_4. With the help of these diagrams, the molar volume and composition of fluid inclusions can be derived directly from T_m and T_h data. The accuracy of the diagrams (besides for CO_2–CH_4 also constructed for CO_2–N_2 and CO_2–H_2S, etc.) has been improved by new experimental data and the development of more accurate equations of state. Furthermore, the compositional and volumetric ranges of application could be extended and cover now the properties of most natural fluid inclusions. The phase transitions in carbonic inclusions with more than 20 mol% CH_4 and/or N_2 in the mixture deviate considerably from 'pure' fluids (Guilhaumou et al., 1981; Van den Kerkhof, 1988). In this paper, an overview of most important phase behavior of gas mixtures in fluid inclusions is given. It is shown that the phase behavior during microthermometry runs is uniquely given for any possible combination of molar volume and composition.

2. Phase transitions in pure gas inclusions

Contrary to water, carbonic inclusions show phase transitions always at lower temperatures than the geological conditions at which they are formed. Above 31.1°C (the critical temperature of CO_2), gas inclusions are always in a supercritical state and essentially monophase. This means that phase separation at geological conditions is unimportant as far as water is not considered. Aqueous inclusions are normally heated in order to study the phase behavior of fluid inclusions at the conditions of trapping; on the contrary, phase transitions in gas inclusions can be studied only at low temperature, far from geological conditions, in order to determine the physical properties of the fluid.

2.1. The system CO_2

Fig. 2 shows the system CO_2 as a *PT* projection. The main elements of the system are three univariant curves for coexisting LG, SL and SG; these curves separate the three phase stability fields for solid (S), liquid (L) and gas (G). The boiling point curve (in fluid inclusion terminology also referred to as the homogenization point curve) represents the *PT* conditions of coexisting liquid and gas phases (LG) ending up in the critical point (CP) at which the properties of liquid and gas become equal (L = G). The density (d) of critical CO_2 is 0.466 g/cm^3, or the molar volume (V) is 94.44 cm^3/mole as calculated from the expression $V = M/d$, where M is the molecular mass (= 44 for CO_2). It is noted that the density and molar volume are expressions of essentially same fluid properties and can be at any time transformed one towards the other. We will see, however, that for fluid mixtures, the use of the molar volume is much more practical.

Along the steep melting point line (SL) in Fig. 2, the solid and liquid phases are in equilibrium. The high pressures of the melting line are only reached in fluid inclusions of very high density/low molar volume (see later). The sublimation curve defines the conditions of coexisting solid and gas (SG). The three stability curves (LG, SL, SG) intersect in an invariant triple point (at -56.6°C and 5.18 bar) where the three phases coexist. The density (d) of the liquid in the triple point is 1.17 g/cm^3 (or V is 37.35 cm^3/mole). Pure CO_2 inclusions with densities lower than 1.17 g/cm^3 (in practice, almost all CO_2 inclusions except very-high density ones) melt at conditions defined by the triple point.

The principle phase transitions in CO_2 inclusions are schematically illustrated in Fig. 2.

A fluid inclusion with $0.466 < d < 1.17$ g/cm^3 (or $37.35 < V < 94.44$ cm^3/mole) is trapped and

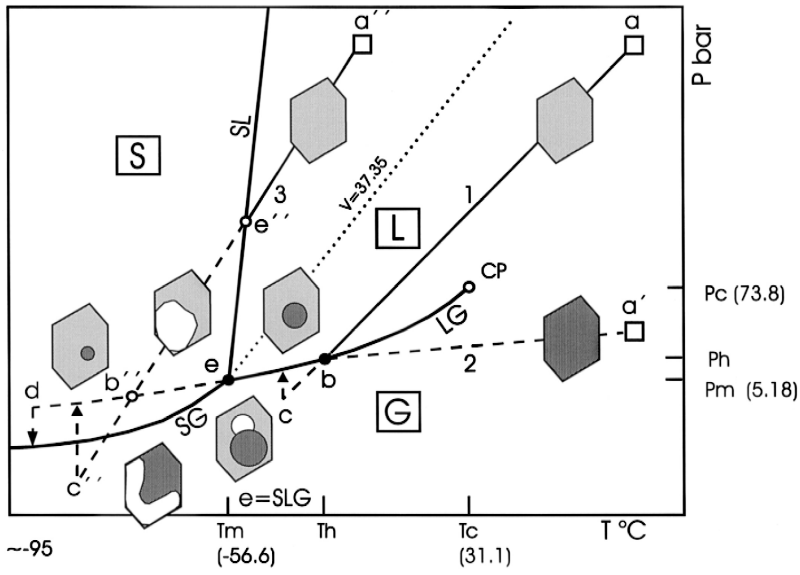

Fig. 2. Schematic *PT* diagram showing phase transitions for inclusions trapped at a, a′, and a″ (see text for explanation). Fillings in the fluid inclusion icons: dark gray = gas phase; light gray = liquid; white = solid phase.

closed at *PT* conditions given by point a. On cooling, the fluid pressure in this inclusion is defined by the isochore 1. The isochore is the graphical presentation of the equation of state expressed for constant volume. Reaching the *PT* conditions on the boiling point curve (b), phase separation is expected, however, about 5° of undercooling below this point is normally necessary in order to nucleate the bubble. In this temperature range, the liquid phase is metastable and the pressure drops below the boiling point curve by following the metastable extension of the isochore. Bubble nucleation (point c) causes a sudden pressure rise resulting in *PT* conditions plotting on the boiling point curve (LG). As the rates of undercooling are not reproducible, phase transitions (homogenization and also the melting temperature) are normally measured only on warming. After bubble nucleation, the temperature of bubble disappearance (T_h) homogenization to the liquid phase (LG → L) can be measured (point b). On further warming, the liquid field is entered and *PT* conditions defined again by the isochore 1. The homogenization temperature directly defines the fluid inclusion density, which can be obtained from Fig. 3, based on the tables of Angus et al. (1976b).

In the example described above, homogenization is to the liquid phase (bubble shrinkage). Low-density inclusions (< 0.466 g/cm^3 for CO_2) show homogenization to the gas phase (bubble expansion until only gas remains: LG → G). The latter case is illustrated by the inclusion trapped at *PT* conditions a′ (Fig. 2). Above the homogenization temperature, the pressure of this inclusion is defined by isochore 2. Fluid inclusions with critical density (0.466 g/cm^3 or $V = 94.44$ cm^3/mole) show homogenization characterized by a fading meniscus without bubble contraction or expansion in the CP at 31.1°C. As the properties of liquid and gas are very similar at these conditions, homogenization at slightly lower temperatures than critical typically shows drastic changes of the bubble volume. Due to similar densities of liquid and gas in fluid inclusions of sub-critical density, ‘bouncing’ bubbles due to pseudo-Brownian movements are common (see Roedder, 1984) and can be used as a criterion to recognize a near-critical state of the fluid. Otherwise, this phenomenon can be observed near the temperature of homogenization (to liquid) in most CO_2 inclusions.

In order to measure the melting temperature, the inclusions (in the examples shown in Fig. 2, both

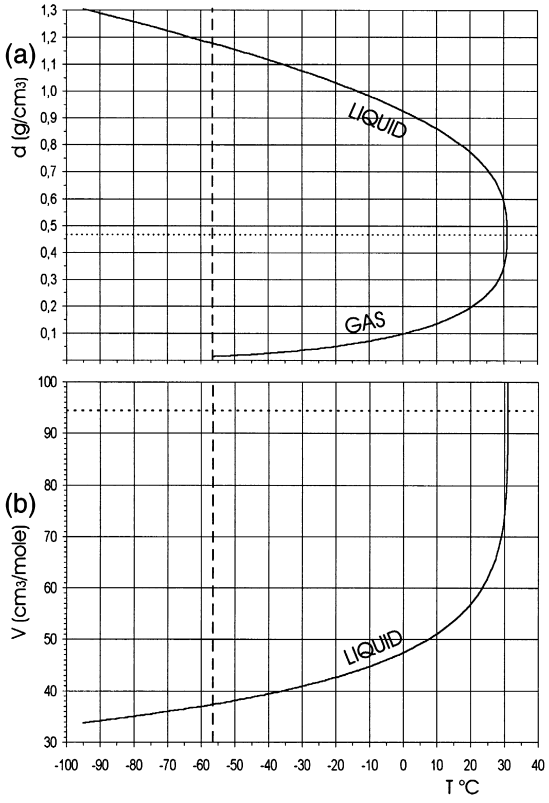

Fig. 3. (a) Densities of the liquid and gas phases on the boiling point curve as a function of temperature (b) The molar volume of the liquid phase on the boiling point curve as a function of the temperature.

inclusions trapped at a and a′) are cooled to temperatures in the order of −95°C, i.e. about 40°C below the triple point (−56.6°C) due to the lag of nucleating solid CO_2. *PT* conditions follow the metastable extension of the boiling point curve below the triple point. The nucleation of the solid phase (point d) is characterized by a sudden pressure drop, which adjusts to that defined by the sublimation curve (SG). During subsequent warming, the *PT* conditions follow the sublimation curve up to the triple point (e). At this temperature, a liquid forms resulting in a three-phase equilibrium (SG → SLG). The solid phase melts and the liquid fills up a part of the inclusion cavity until only the liquid and gas phases remain (SLG → LG). At temperatures above the triple point, the boiling point curve is followed up to the temperature of homogenization.

CO_2 inclusions with a very high density of > 1.17 g/cm^3 (molar volume < 37.347 cm^3/mole) have been described in mantle xenoliths (Frezzotti et al., 1992; Andersen and Neumann, 2001) and in migmatite (Van den Kerkhof and Olsen, 1990). These inclusions show a slightly different phase behavior compared to the examples given above (inclusion trapped at a″ in Fig. 2): homogenization takes place along the metastable extension of the boiling point curve below the triple point (see also Swanenberg, 1980, pp. 22–23). Melting is characterized by the phase transition SL → L and occurs around −52°C on the melting curve with positive slope, at some degrees centigrade higher than the triple point. It is often difficult to observe this melting due to the similar refractive indices of both solid and high-density liquid. The use of a low position of the condenser and small diaphragm is recommended. During cooling, the *PT* conditions of an inclusion trapped at a″ (Fig. 2) follow isochore 3, including the metastable extension of the isochore at lower temperatures. Not any phase transition can be observed until reaching point c″ (bubble nucleation). On subsequent warming, homogenization (LG → L) takes place at the intersection point (b″) of the metastable boiling point curve and the metastable part of isochore 3. When the inclusion is first cooled until point d (solid nucleation), the sublimation curve (SG) is followed up to the triple point, like for lower density inclusions. However, in the present case of very high density, not the solid but the bubble disappears at −56.6°C resulting in a solid + liquid equilibrium on further warming (SLG → SL). Conditions follow the melting point line up to point e″ (solid melting). At higher temperatures, the liquid field is entered (SL → L) and the fluid pressure defined by the isochore 3.

The intent of measuring the melting temperature of carbonic inclusions is to check the purity of the CO_2: additional components like CH_4 and N_2 will lower the melting temperature down to −61°C for CO_2–N_2 and to much lower temperatures for CO_2–CH_4.

2.2. The one-component systems CH_4 and N_2

Both CH_4 and N_2 inclusions are characterized by very low homogenization temperatures, i.e. below

the respective critical temperatures of −82.6°C (CH_4) and −147.0°C (N_2). Molar volumes of pure fluids can be directly obtained from the *VT* properties of the boiling point curve for each component (e.g. Angus et al., 1976a, 1979). Measuring the melting temperature with regular microthermometry equipment (cooled with liquid nitrogen) is difficult, but sometimes successful for CH_4 inclusions (−182.5°C). In our experience, CH_4 inclusions can be frozen only by using a gas-flow stage, where liquid nitrogen with a temperature of −196°C flows directly over the sample at the lowest temperatures. Nitrogen inclusions ($T_m = -210.0$°C) cannot be frozen by using regular cooling equipment. Attempts of freezing fluid inclusions with helium as an alternative cooling agent (−269°C) are unusual due to the technical complications and high costs. Kreulen and Schuiling (1982) could reach temperatures as low as −240°C in this way. Fig. 1b and c shows CH_4 and N_2 isochores for different molar volume and homogenization temperatures.

3. The binary systems CO_2–CH_4 and CO_2–N_2

Carbonic fluid inclusions, which are not pure in composition in most cases, can be considered as binary or pseudobinary mixtures of CO_2–CH_4 or CO_2–N_2. Fig. 4 shows the main elements of a *PT* phase diagram for the system CO_2–CH_4 including phase transitions of a fluid inclusion with about 30 mol% CH_4 and molar volume of about 50 cm^3/mole. Compared to the pure systems (cf. Fig. 2), additional forms appear in these phase diagrams: the ternary solid–liquid–gas (SLG) phase equilibria and the critical conditions (L = G) are both presented by curves (Fig. 4). As shown by the phase rule, the insertion of one component in a system adds one additional degree of freedom. As a consequence, any invariant point in the phase diagram of a pure fluid system is transformed into univariant curves for binary mixtures. In the same way, previous univariant objects for one-component system become divariant for two-component systems. This is the case of the liquid–gas (LG) association, which goes from an univariant curve in the *PT* phase diagram of pure systems to a bivariant surface for binary mixtures in the *PTX* space. This surface delimits the *PTX* field, where the system is monophasic, from the field where the system is diphasic. As a matter of fact, divariant phase associations (i.e. surfaces) can only be represented on a sheet of paper by fixing one parameter, for example, the composition. Such an operation yields a curve called the 'isopleth'. One of these isopleths is illustrated in Fig. 4 and is composed of two parts called the bubble point and the dew point curves, respectively. The bubble point curve marks the *PT* conditions, for which an infinitesimally small amount of gas is present in the liquid and is going to appear (or disappear). On the contrary, the dew point curve indicates the *PT* conditions, for which only a tiny amount of liquid is present in a gas. The bubble and dew point curves meets at a CP (L = G). Thus, the critical curve intersects the isopleth at this point. As expected, both the dew and bubble point curves end at lower temperatures against the univariant SLG curve, indicating the stability of the solid phase. The phase diagram, presented here for a binary system, allows the interpretation of phase transitions observed in fluid inclusions. Let us consider the case of a CO_2–CH_4 fluid inclusion, which is monophasic at high temperature (point a), but as usual, because of nucleation problems, it is better to describe the phase transitions by starting from low temperatures. At very low temperatures, this fluid inclusion is in a diphasic state with solid and gas. With increasing temperatures, the pressure accordingly increases, and at point i, the isochoric path of the inclusion intersects the SLG curve at temperature T_i. This point marks the beginning of the condensation of a liquid on the walls of the inclusion. Then, as long as the ternary SLG phase association is present in the fluid inclusion, the isochoric path follows a part of SLG curve, characterized by dropping pressures, until the complete disappearance of the CO_2 solid at point m (the melting temperature T_m). From this point, the inclusion contains now a biphasic liquid–gas assemblage, which goes to higher pressures with increasing temperatures. The size of the gas bubble progressively diminishes until the homogenization point (point b, temperature T_h), where the gas bubble completely disappears. Then, the inclusion follows its isochoric path (denoted as isochore 1 in Fig. 4) until point a. Low-density fluid inclusions with the same bulk composition may homogenize to gas at the same

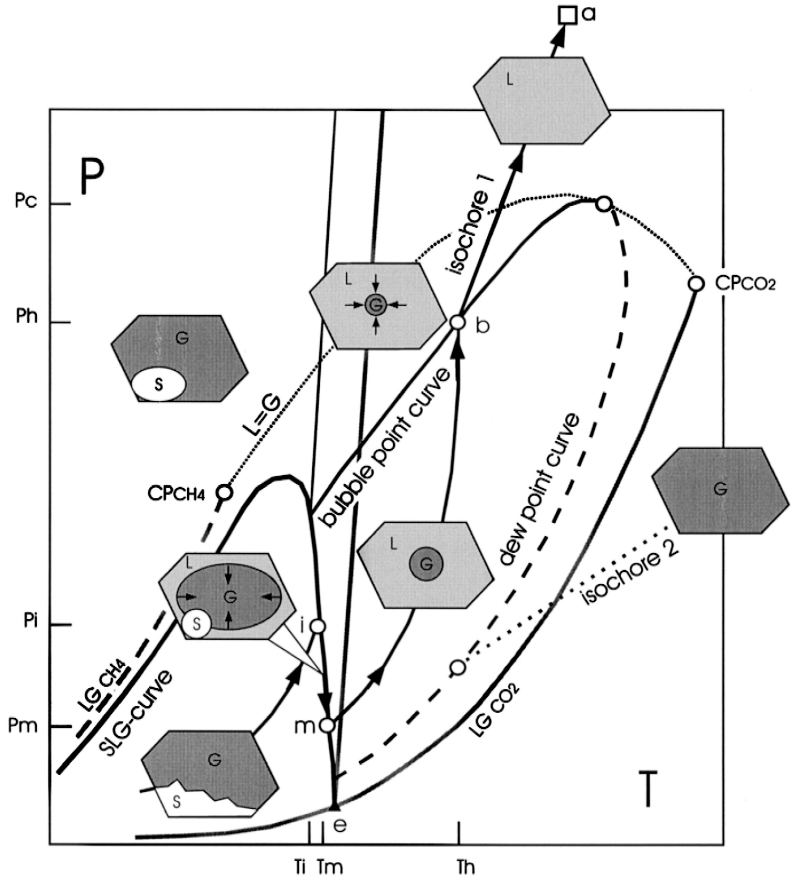

Fig. 4. Schematic *PT* phase diagram of the binary system CO_2–CH_4 showing phase changes along the heating path. Thick gray dashed line (LG_{CH_4}) = the saturation curve of CH_4; thick gray line (LG_{CO_2}) = the saturation curve of CO_2. Univariant curves: dotted line (L = G) = the critical curve, connecting the two CPs of the pure CO_2 and CH_4 components; thick solid line = the SLG or melting curve (see text for further explanation).

temperature: their isochoric path is defined by the line denoted as 'isochore 2' (Fig. 4), which ends at T_h on the dew point curve.

The topologies of the CO_2–CH_4 and CO_2–N_2 systems are illustrated in Fig. 5. The systems mainly differ by the different relative positions of the three-phase (SLG) and critical curves (L = G): both lines are continuous for the system CO_2–CH_4, but intersect for CO_2–N_2. Consequently, the critical curve is continuous between the two CPs of the pure components for the system CO_2–CH_4 but is discontinuous for the system CO_2–N_2.

In the system CO_2–CH_4 (Fig. 5a), a second critical curve delimits the co-existence of two metastable liquids (mL = L, where 'm' denotes metastable phases) or mL = LG phase assemblages. The critical L = G and mL = L curves do not intersect, which results in a 'type II' topology for the system CO_2–CH_4 according to the terminology of Van Konynenburg and Scott (1980). Immiscibility of two liquids, i.e. a double meniscus, can be observed in CO_2–CH_4 fluid inclusions of intermediate composition and higher density at temperatures below −83°C, just before solid nucleation, which normally takes place between −85°C and −105°C (Berdnikov, 1987; Van den Kerkhof et al., 1993; Thiéry et al., 1994b). In these inclusions, additional, metastable phase transitions can be found: LL → L (liquid–liquid homo-

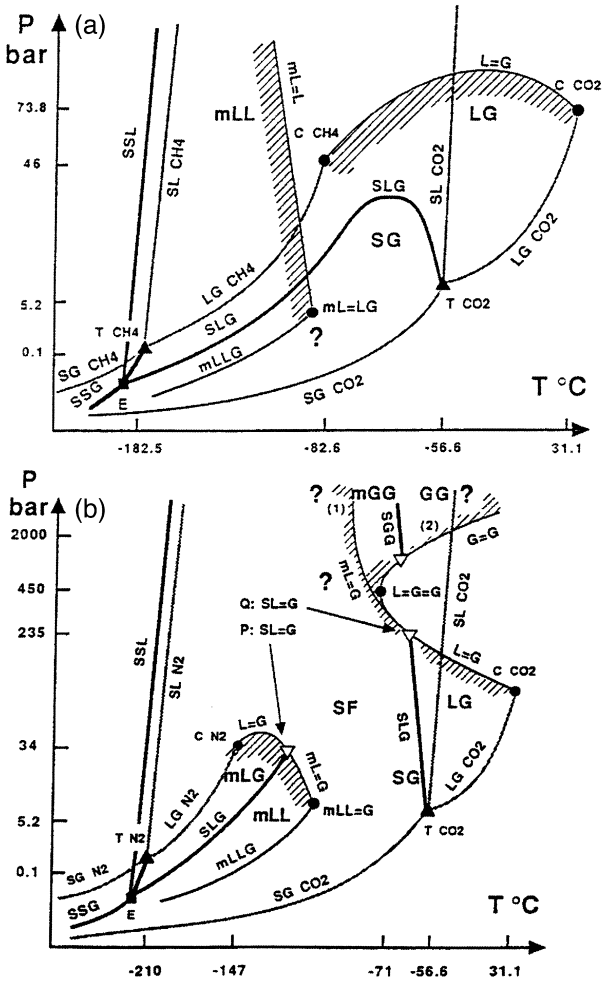

Fig. 5. Topology of the systems CO_2–CH_4 (a) and CO_2–N_2 (b), after Thiéry et al. (1994b). The pressure and temperature scales are arbitrary. Invariant points: eutectic point (E, filled square), triple points (T, filled triangles), L = G CPs for pure fluids (C, filled circles), three-phase critical end-points (filled circles), SL = G intersection points of a critical curve with the SLG curve (triangles). Univariant lines: two-phase assemblage for the pure end-members (gray lines), three-phase assemblage for the binary systems (thick solid lines), and critical curves (thin solid lines). The prefix 'm' denotes metastable parts. Regions around the triple points T_{CH_4} and T_{N_2} are enlarged. The critical curves (L = L and L = G) delimit LL and LG immiscibility (shaded areas). Also indicated are the stability fields of liquid–liquid (LL), solid–gas (SG) and solid–fluid (SF). The calculated extensions of the critical curve towards high pressures for CO_2–N_2 are sketched according to (1) Thiéry et al. (1994b) and (2) Kreglewski and Hall (1983). The pressure and temperature scales are arbitrary.

genization), LLG → LG (partial liquid homogenization) and rarely LLG → LL (partial liquid–gas homogenization).

In the system CO_2–N_2 (Fig. 5b), the critical curve (L = G) is intersected twice by the SLG curve. At the intersection points (P and Q), solid is in equilibrium with critical fluid (denoted as SL = G). The lower temperature intersection point (P) is very close to the CP of pure N_2, whereas the intersection point at the high temperature side (Q) has been localized at about 235 bar, $X_{N_2} = 0.47$ and $T = -61.2$°C (Van den Kerkhof, 1990). At these conditions, critical homogenization and melting take place at the same temperature. The discontinuity of the L = G critical

curve results in 'type III' topology (Van Konynenburg and Scott, 1980). The (partly metastable) extension of the critical curve beyond point Q to higher pressure is not exactly known (possibilities (1) and (2) in Fig. 5b). However, recent experiments by Kooi et al. (1998) show that a critical double point (L = G = G) suggested by possibility (2) in Fig. 5b and defining a field of fluid–fluid immiscibility based on predictions of Kreglewski and Hall (1983) is not realistic. This result is consistent with calculations of Thiéry et al. (1994b), which can be applied down to the temperature of solid nucleation.

3.1. The consequence of retrograde condensation for phase transitions at constant volume

The experimental data of Arai et al. (1971) for CO_2–CH_4 and CO_2–N_2 already showed that — contrary to pure systems — LG-immiscibility is possible in mixtures above the critical temperature. This phenomenon is a consequence of retrograde condensation, i.e. the condensation of liquid on lowering pressure (and volume expansion). The implication of retrograde condensation for fluid inclusions is that, for a given composition, homogenization (always to the gas phase) can be observed at higher temperatures than critical. For example, in synthetic fluid inclusions, Van den Kerkhof (1988) found gas homogenization as high as 12°C for CO_2–N_2 with 25% N_2, although the critical temperature for this mixture is about 7°C. On the other hand, homogenization to liquid is always below the critical temperature.

Retrograde condensation behavior results in significantly higher degrees of fill, compared to fluid inclusions showing 'normal' gas homogenization (and the same composition) (Thiéry et al., 1994b). The effect is particularly important for the system CO_2–N_2. Gas homogenizations in mixtures are not necessarily indicative for low densities, but may also indicate high-density mixtures. Actually, the fact that gas homogenization is frequently recorded for gas mixtures can be explained the effect of retrograde condensation: this type of homogenization can be much more easily observed compared to 'normal' gas homogenization of lower-density fluid inclusions. The latter can be observed only with difficulty due to the optical restrictions of observing small amounts of liquid (< 10 vol.%). An implication of retrograde condensation is that two fluid inclusions of the same composition, but different densities, may show the *same* homogenization temperature.

4. *VTX*-phase diagrams

Current diagrams mostly show projections of pressure (P), temperature (T), and composition (X), i.e. isopleths (constant X) in a PT diagram. However, fluid inclusions have *constant volume* (V) and *constant bulk composition* (X) whereas the temperature and pressure are variable; the pressure cannot be directly determined in fluid inclusions. Therefore, an alternative type of phase diagrams has been proposed which basically represents projections of the molar volume (V), the temperature (T) and the composition (A). Most useful for the interpretation of fluid inclusions appeared to be *TX* and *VX* diagrams. The isochoric *TX* diagram has the advantage that the phase fields can be presented for constant total volume. Furthermore, microthermometry and Raman data, i.e. temperatures and compositions, can be directly plotted. The *VX* diagram (Burruss, 1981) has the advantage that both V and X can be read from the diagram by plotting *microthermometry data* only (crossing isotherms); in this case, quantitative Raman analysis can be used as an independent check. Examples of both *TX* and *VX* diagrams for the systems CO_2–CH_4 and CO_2–N_2 are discussed below.

5. Isochoric sections of the binary *TX* diagram

For CO_2-rich inclusions with less than 20 mol% of other gas compounds, it is mostly impossible to distinguish between CO_2–CH_4 or CO_2–N_2-dominated mixtures without additional Raman analysis. However, for fluid inclusions with > 80 mol% of N_2 or CH_4, the phase behavior is directly indicative for one of the two systems. These differences are illustrated by the phase diagrams shown in Fig. 6.

The principle forms in the diagrams are (1) the melting and sublimation curves, (2) the homogeniza-

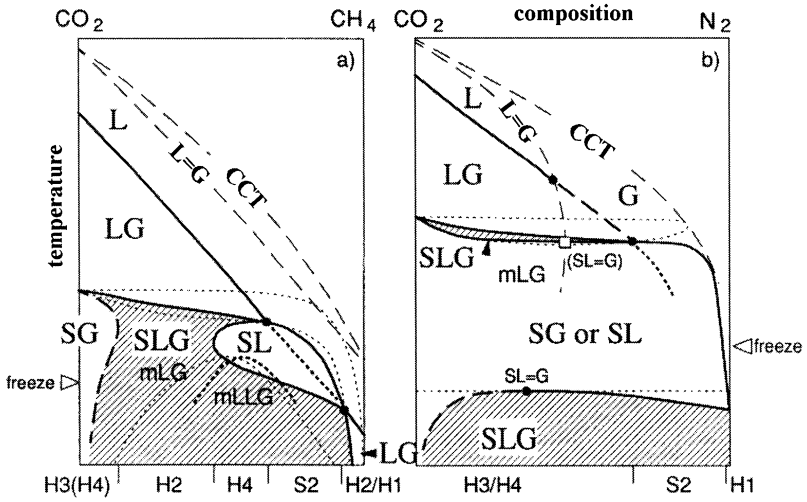

Fig. 6. Topology of isochoric *TX* diagrams (molar volume ~ 50 cm^3/mole) for the systems CO_2–CH_4 and CO_2–N_2. Shaded area shows the stability of coexisting SLG. L = G is the (polychoric) critical curve; CCT is the 'cricondentherm', the maximum extension of the LG-immiscibility (see text for explanation).

tion point curve and (3) the partial homogenization (SLG → SL), and initial melting curves (SL → SLG). The homogenization temperatures are drastically lowered for higher CH_4 or N_2 contents, whereas melting temperatures are lowered only some degrees. As a consequence, the homogenization and the melting curves intersect towards higher CH_4 or N_2 concentrations between about −70°C and −56.6°C (except for molar volumes between about 58 and 160 cm^3/mole for CO_2–CH_4, but *always* for the system CO_2–N_2). Fluid inclusions with compositions plotting left of the intersection point show $T_h > T_m$; fluid inclusions with compositions plotting right of the intersection point show $T_h < T_m$. For the latter inclusions, homogenization of the metastable liquid and gas plot on the extension of the homogenization point curve below the melting point curve (stippled lines in Fig. 6).

Fluid inclusions of the same molar volume but different composition may show liquid homogenization for CO_2-rich composition, but gas homogenization for higher CH_4 or N_2. This is illustrated in Fig. 6b by the intersection of the homogenization point curve (for constant molar volume) and the critical curve (L = G). Homogenization to the gas phase typically shows a 'retrograde condensation' behavior meaning that liquid fill degrees below homogenization are extraordinary large. The field of 'retrograde condensation' fluids is limited by the cricondentherm (CCT) in Fig. 6. The CCT is defined here as the maximum extension of the LG-immiscibility field.

On cooling to very-low temperatures (about −180°C), three phases (SLG) are stable in both CO_2–CH_4 and CO_2–N_2 systems (shaded areas in Fig. 6). However, at the freezing point (normally around −95°C; see temperatures indicated as 'freeze' in Fig. 6), CO_2–CH_4 inclusions cannot be frozen completely and a liquid phase (even when the amount is small) always remains after solid nucleation; CO_2–N_2 inclusions can be frozen completely (SG), i.e. without leaving a liquid phase behind. The principle reason for this behavior is the higher solubility of CH_4 in CO_2–rich fluids. In the phase diagram, the three-phase field is continuous for CO_2–CH_4, but split into two domains for CO_2–N_2. In the latter system, two points are defined where solid CO_2 is in equilibrium with critical fluid (SL = G). For the compositional range denoted as 'H4' in the system CO_2–CH_4 (see later) at rising temperature, the bubble disappears when entering the SL field (SLG →

SL) and re-appears at higher temperature (SL → SLG), followed by final melting and homogenization.

6. The interpretation of microthermometry data: the application of *VX* diagrams

VX diagrams are highly powerful for the interpretation of microthermometry data as the bulk *VX* properties (as well as the *VX* properties of the individual phases) can be directly deduced from phase transition temperatures. Additional Raman analysis (qualitative or quantitative) is not always essential as far as the system is known. The *VX* diagram was popularized by Burruss (1981) for the application to fluid inclusion studies and several diagrams have been published since then by compilation of experimental data and by application of different equations of state: Heyen et al. (1982) and Herskowitz and Kisch (1984) for CO_2–CH_4, Darimont and Heyen (1988) for CO_2–N_2 and Van den Kerkhof (1990) and Thiéry et al. (1994a,b) for both systems.

The topologies of the *VX* diagrams for CO_2–CH_4 and CO_2–N_2 are shown in Fig. 7. At a constant temperature, each phase is shown as a point in the diagram with the coexisting phases connected by tie-lines. For the three-phase SLG equilibria at a given temperature, the liquid and gas phases plot as points in Fig. 7: liquid in equilibrium with solid and gas [L(SG)] and gas in equilibrium with solid and liquid [G(SL)]. The loci of *VX* properties for the liquid and gas phases in three-phase equilibrium (at different temperatures) are indicated by the stippled lines. The solid phase in the binary CO_2–CH_4 and CO_2–N_2 systems is always pure CO_2 ($V = 28.2$ cm^3/mole) and therefore always plots at the same point. A fluid inclusion containing SLG plots within the triangle formed by the three apices for the *VX* properties of liquid, gas and solid. If one of the three phases disappears on changing temperature, the fluid inclusion must plot on the tie-line, which connects the two remaining phases. For example, in the case of final melting (SLG → LG), the bulk *VX* properties of the inclusion should plot on the tie-line denoted as LG(S) in Fig. 7. This tie-line divides the SLG and the LG-fields.

Homogenization to liquid (LG → L) is possible below the critical curve (L = G) shown for CO_2–CH_4

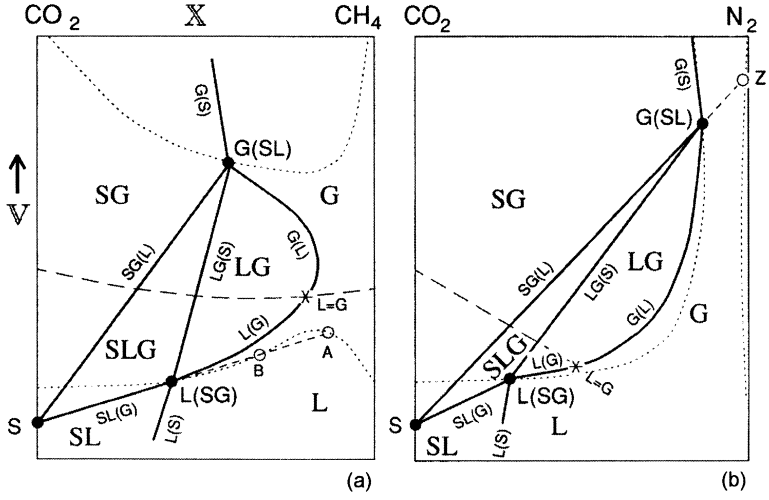

Fig. 7. The topology of isothermal *VX* diagrams for the systems (a) CO_2–CH_4 and (b) CO_2–N_2. Stippled curves present the loci of the univariant (polythermal) SLG equilibria for the liquid and gas phases. The dashed lines are the critical curves (L = G). Solid lines delimit the phase fields. The SL(G)-curves for different temperatures may in part coincide and represent both partial homogenization, initial melting or bubble nucleation for the same fluid inclusion: e.g. for CO_2–CH_4 the tie-line S–A represents coexisting solid and liquid at the transition SLG → SL (partial homogenization), tie-line S–B at the transition SL → SLG (bubble nucleation), and tie-line S–L(SG) at the transition SLG → LG (final melting). Equally for the system CO_2–N_2 the tie-line S–Z represents the properties of solid and gas at the transition SLG → SL or SLG → SG (partial homogenization), the tie-line S–G(SL) the same properties at the transition SG → SLG (initial melting).

and for CO_2–N_2 (dashed lines in Fig. 7). Above the critical curve (higher V), homogenization is to the gas phase. Similarly, for CO_2–N_2, partial homogenization to liquid (SLG → SL) is found below the line representing solid in equilibrium with critical N_2 (SL = G); partial homogenization to gas (SLG → SG) is found above this line. CO_2–N_2 fluid inclusions plotting under the SL = G line and above the L = G curve show partial homogenization to the liquid below −147°C and gas homogenization before −32°C during subsequent warming (Fig. 10). Between curves L = G and the CCT (Fig. 8), homogenization is to the gas phase showing 'retrograde condensation' behavior meaning that liquid fill degrees are large compared to 'normal' gas homogenization.

In Fig. 8a and b, line 1 (in both diagrams) indicates fill degrees of 10% liquid: the liquid phase in inclusions plotting above these lines normally cannot be observed due to the optical restriction of observing small amounts of liquid. CO_2–CH_4 inclusions plotting below line 2 (Fig. 8a) cannot be frozen completely and always contain a CH_4-rich liquid after solid nucleation; inclusions plotting above line 2 show phase behavior similar to that of pure CO_2 inclusions. Inclusions plotting below line 3 in Fig. 8a may show bubble nucleation (SL → SLG) on warming. For CO_2–N_2 inclusions plotting below line 4 (Fig. 8b), partial homogenization can be observed below −147°C; inclusions plotting above this line do not show visible partial homogenization and look similar to pure CO_2 inclusions. Inclusions plotting above line 1 and above line 4 do not show any visible phase transition and appear 'empty', except for a small amount of solid, which may form after sublimation. However, solid particles in low-density inclusions have been observed only in few cases and are assumed to be not at all observable when their V–X-points plot at the right of line 5 (Fig. 8b) delimiting the 1 vol.% solid for SG equilibria.

Example 1 (CO_2–CH_4) (Fig. 8a). The VX properties of fluid inclusion A ($V = 48$ cm^3/mole; $X_{CH_4} = 0.25$) are defined by the cross-cutting isotherms for (1) homogenization to liquid (LG → L) at −20°C shown by the curve L(G) and (2) final melting (T_m) at −62.5°C shown by the dashed-pointed line LG(S).

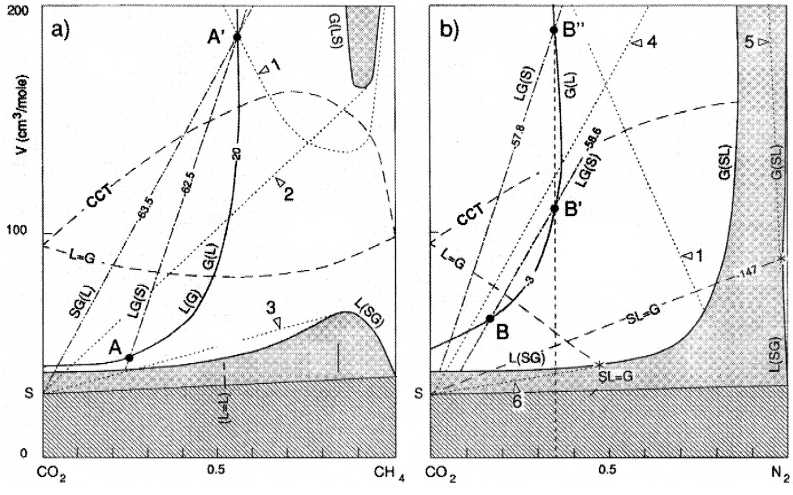

Fig. 8. The use of VX diagrams for the determination of molar volume and composition from microthermometry data (from Thiéry et al., 1994b). Thick solid line: L(SG) and G(SL) curves. Inclusions plotting in the shaded area are characterized by '$T_h < T_m$', in the non-shaded by '$T_h > T_m$'. Inclusions plotting below the critical curve (L = G) homogenize to liquid, above the critical curve to gas. Inclusions between the curve denoted as CCT ('cricondentherm' or second-order critical curve) and L = G show homogenization to gas at higher temperature than critical for a given bulk fluid composition as a consequence of retrograde condensation. Line signatures for the phase transitions are the following: thin solid lines = homogenization (LG → L or LG → G); dashed-dotted lines = final melting (SLG → LG); dashed-double dotted lines = initial melting (SG → SLG), bubble nucleation (SL → SLG) or partial homogenization (SLG → SG or SLG → SL) (see text for further explanation).

Inclusion A′ has the same T_h and T_m as for inclusion A, but homogenization is to the gas phase (LG → G). As an additional phase transition, initial melting (T_i) can be observed at −63.5°C for inclusion A′.

Example 2 (CO_2–N_2) (Fig. 8b)). Inclusion B (V = 53 cm^3/mole; $X_{N_2} = 0.15$) shows homogenization to liquid (LG → L), indicated by the curve G(L) at −3°C, and final melting (SLG → LG), indicated by the line LG(S) at −58.6°C. As B plots above the SL = G line, partial homogenization must be to the gas phase (SLG → SG) at −153°C (line not shown). The temperature difference between initial and final melting is very small (lines for initial melting are omitted in Fig. 8b). Homogenization and melting temperatures for inclusion B′ are the same as for inclusion B, but homogenization is to the gas phase.

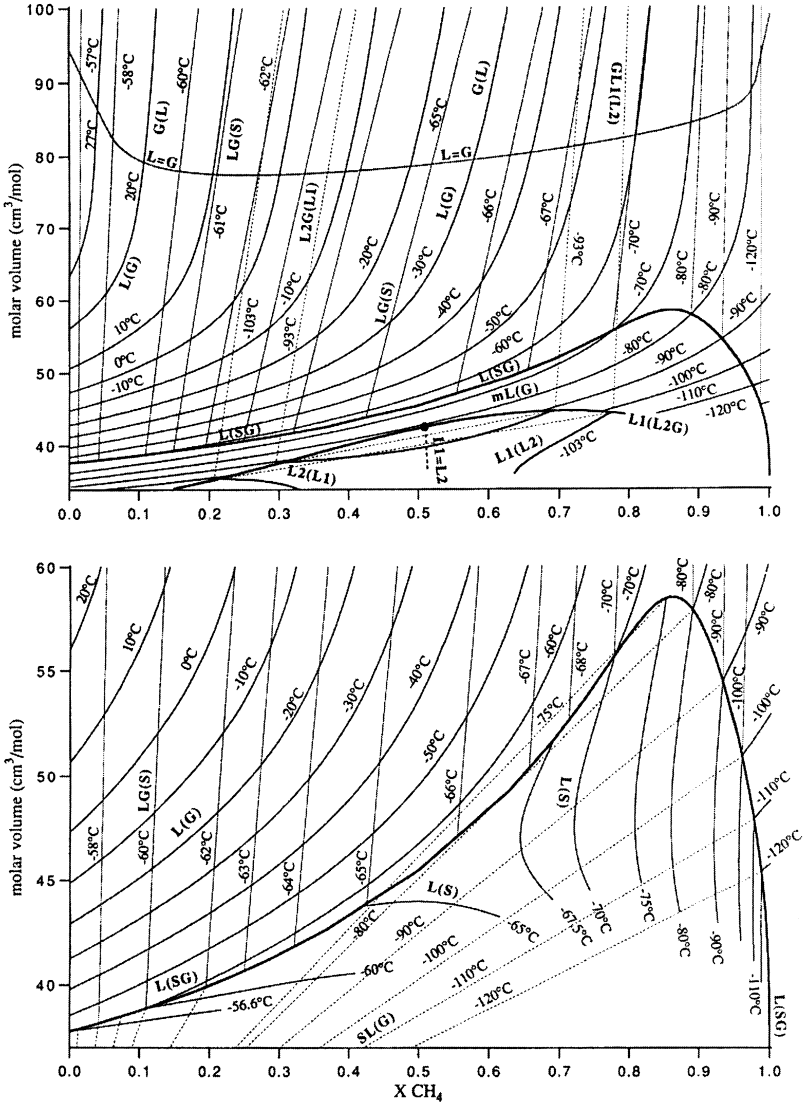

Fig. 9. *VX* diagrams calculated for the system CO_2–CH_4 for (a) $V < 100$ cm^3/mole and (b) for $V < 60$ cm^3/mole (from Thiéry et al., 1994b).

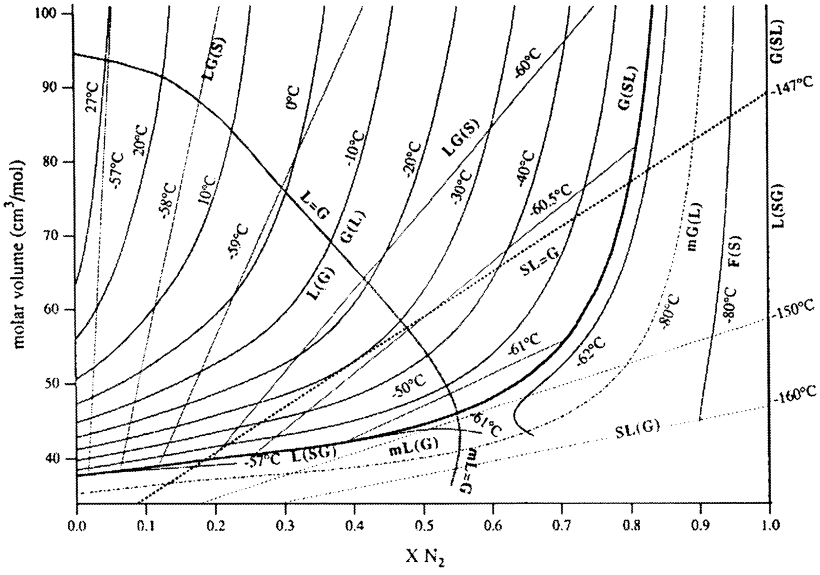

Fig. 10. *VX* diagram calculated for the system CO_2–N_2 for $V < 100$ cm^3/mole (from Thiéry et al., 1994b).

As B′ plots in the field delimited by the curves L = G and CCT, the fluid inclusions shows 'retrograde condensation' behavior. Inclusion B″ shows homogenization to gas phase at the same temperature as for inclusion B′, but melting takes place at higher temperature (−57.8°C) and liquid fill degrees are much lower. Comparison of the inclusions B′ and B″ shows that inclusions of the same composition, but different molar volume may have the *same* homogenization temperature. In practice, however, observed gas homogenization almost always represents the higher density inclusion, i.e. the one characterized by 'retrograde condensation' behavior.

Figs. 9 and 10 show *VX* diagrams for the systems CO_2–CH_4 and CO_2–N_2 as calculated by the Soave–Redlich–Kwong equation of state combined with the Lee–Kesler correlation (Thiéry et al., 1994b). These diagrams can be used to directly determine the *VX* properties of fluid inclusions by plotting microthermometry data: the *VX* properties are fixed for given two phase transition temperatures, usually, but not necessarily the homogenization and melting temperatures (T_h; T_m). Also, other temperature combinations like for high-density CO_2–CH_4 inclusions partial homogenization (SLG → SL; stippled lines SL(G) in Fig. 9b) and solid dissolution (SL → L; solid curves L(S) in Fig. 9b) can be used or sometimes they are the only possible phase transitions.

The sensitivity of determining gas fluid compositions from the melting temperature is much lower for CO_2–N_2: an inclusion of 50 cm^3/mole shows melting point depression of about 1.5°C/10 mol% of CH_4, but only about 0.8°C/10% of N_2. Plotting the combination of partial and normal homogenization temperatures sometimes gives a better result (Fig. 10). Ideally, however, all phase transitions observed in one fluid inclusion can be presented in the *VX* diagrams as lines which all meet in one point, which defines the bulk *VX* conditions of the fluid inclusion.

7. Tracing *VX* properties of the individual phases during microthermometry runs: bubble nucleation in CO_2–CH_4 fluid inclusions as an example

The *VX* diagram can be used also to determine the *VX* properties and relative volume proportions of the individual phases during cooling and warming experiments. Even highly complicated sequences of

phase transitions can be easily reconstructed by graphical methods for any chosen V and X. As an example, we describe below a CO_2–CH_4 inclusion with $X_{CH_4} = 0.60$ and $V = 49$ cm^3/mole (Fig. 11). After freezing (at about -85°C), bubble nucleation (SL → SLG) can be observed during subsequent warming. The complete phase sequence can be described as SLG → SL → SLG → LG → L. This phase behavior has been observed for example in fluid inclusions from migmatitic gneiss from Rogaland, Norway (Van den Kerkhof et al., 1991). The example is remarkable as it demonstrates the possibility of

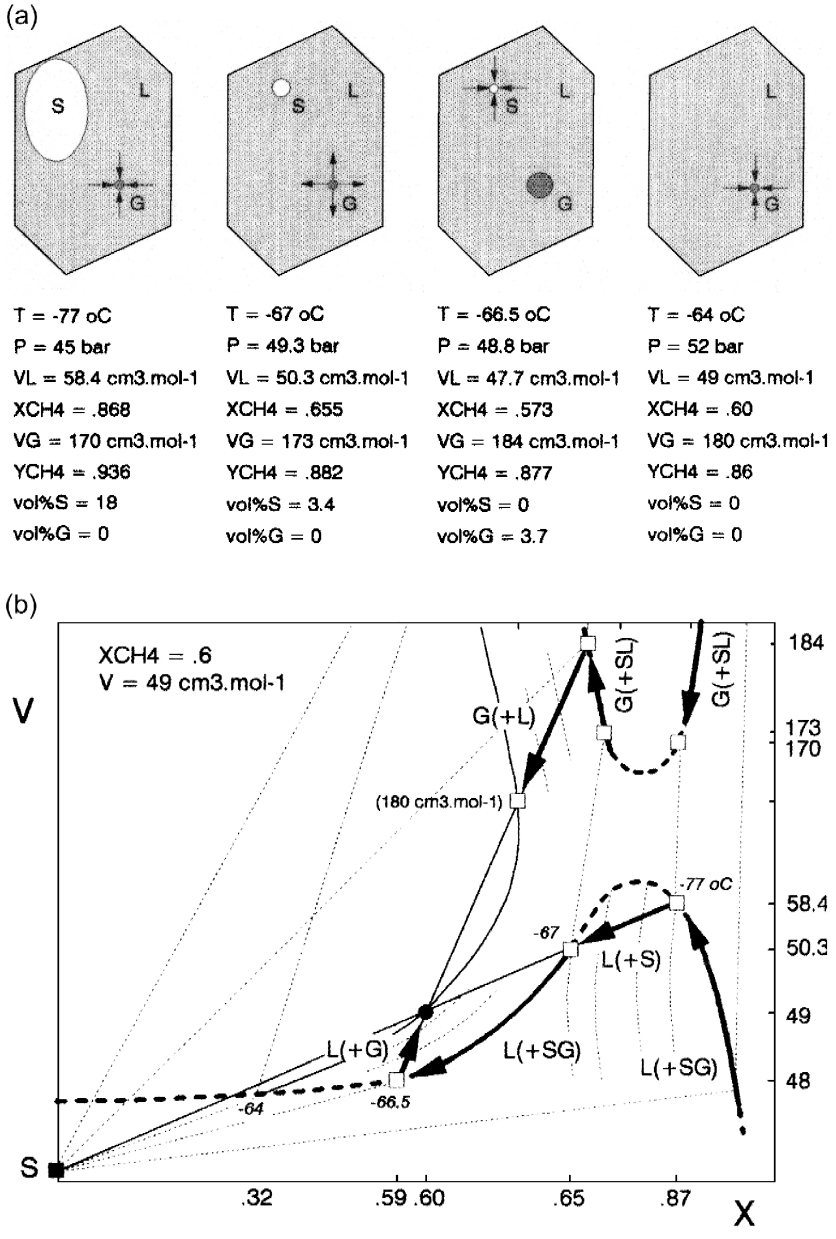

Fig. 11. The molar volume and composition of single phases in CO_2–CH_4 fluid inclusion with bulk properties of $X_{CH_4} = 0.60$ and $V = 49$ cm^3/mole showing the phase sequence SLG → SL → SLG → LG → L (see text for explanation).

nucleating a new phase during warming. Examples of bubble nucleation on warming in other systems (CO_2–H_2O–NaCl) are discussed by Diamond (1996).

Fig. 11 shows that both bubble and solid phases nucleate during cooling resulting in a three-phase equilibrium (solid, liquid and gas) at −100°C. Both liquid and gas phases are CH_4-rich (> 97% CH_4) and almost all CO_2 is partitioned in the solid phase (pure CO_2). During warming, the solid slightly dissolves, and both liquid and gas are enriched in CO_2. At the same time, the molar volume of the liquid increases (lower density), whereas the molar volume of the bubble is reduced (higher density). The bubble shrinks until complete disappearance at −77°C. At this condition, the liquid has increased molar volume to 58.4 cm^3/mole, whereas the molar volume of the last gas bubble has a molar volume of 170 cm^3/mole. The result of partial homogenization is a two-phase (solid and liquid) equilibrium; on further warming *VX* conditions should leave the three-phase curve and enter the SL field. *VX* conditions must follow the tie-line towards point S (*VX* of solid CO_2) in the diagram. The solid further dissolves in the CH_4-rich liquid; X_{CH_4} of the liquid is reduced from 0.87 towards 0.65 (molar volume is lowered from 58.4 to 50.3 cm^3/mole) until a temperature of −67°C is reached. At this point, the liquid becomes immiscible again and a bubble (molar volume of about 173 cm^3/mole) nucleates. The bubble expands on continuing warming during solid CO_2 further dissolves. Like for bubble nucleation on cooling, some overstepping of the temperature is required in order to nucleate the bubble. However, sometimes, metastability may pertain and the bubble does not nucleate before complete melting. After the three phases have once formed the *VX* conditions again follow the three-phase curves (for liquid and gas) in the temperature range between −67°C and −66.5°C until complete solid CO_2 dissolution. In this small temperature range (of about 0.5 degrees) of fast melting, both liquid and gas drastically change composition and molar volume: X_{CH_4} of the liquid is lowered towards 0.59 of the gas phase towards 0.65; the liquid becomes more dense (molar volume decrease from 50.3 towards 48 cm^3/mole) and the gas phase less dense (molar volume increase from 173 towards 184 cm^3/mole). After melting (SLG → LG), the *VX* conditions should follow the tie-line connecting the *VX* conditions of the liquid and gas phase at the melting point. The bubble shrinks on continuing warming until −64°C, the temperature of homogenization (LG → L). The molar volume of the liquid has now become equal to the bulk molar volume of the fluid inclusion (49 cm^3/mole); the molar volume of the last bubble is 180 cm^3/mole.

8. A classification of phase transition sequences: H- and S-type inclusions

The type of phase transitions directly reflects the composition and molar volume (density) of fluid inclusions. The description of complex phase behavior in fluid inclusions can be easily simplified. Van den Kerkhof (1988, 1990) proposed a division in H-type fluid inclusions with $T_h > T_m$ (showing homogenization as the final phase transition) and S-type fluid inclusions with $T_h < T_m$ (showing solid disappearance, i.e. melting or sublimation as the final phase transition on warming), i.e. H-type inclusions are characterized by LG → L or LG → G, S-type inclusions by SG → G or SL → L as the final phase transition. Fluid inclusions within each group (H-type and S-type) show the same *order* of phase transitions in the temperature range normally studied, i.e. from −180°C until 35°C: H-type inclusions show one to four phase transitions of the sequence SLG → SL or SG → SLG → LG → L or G, always including the last transition; S-type inclusions show one to four phase transitions of the sequence SLG → SL or SG → SLG → SL or SG → L or G, also always including the last transition. The phase behavior of every inclusion with compositions of the system CO_2–CH_4–N_2 is uniquely defined by indication of the group (H or S-type), and the *number* of phase transitions (Fig. 12). For example: a fluid inclusion of type H3 (typical for CO_2-rich compositions) shows initial melting (T_i), final melting (T_m) and homogenization (T_h). However, relative phase volumes may be very different within each inclusion type.

Fig. 13 shows the different fluid inclusion types for the ternary compositions in the system CO_2–CH_4–N_2. Type H1 is restricted to CO_2-poor compositions (< about 3% CO_2). Type H2 is typical for

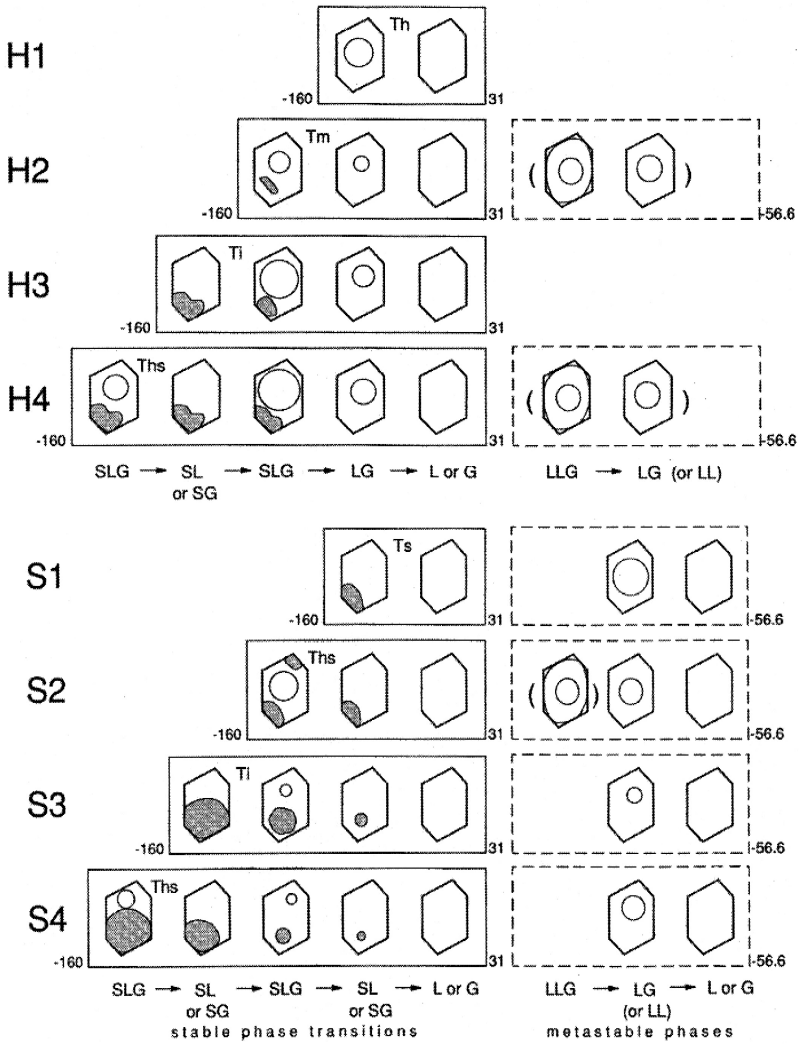

Fig. 12. Sequences of phase transitions in CO_2–CH_4–N_2 inclusions in the temperature range between −160°C and 31°C. Possible metastable transitions (at < −56.6°C) of the undercooled phases are shown at the right. The solid phase is shown in gray; the liquid and gas phases are not filled.

CO_2–CH_4 mixtures and intermediate to high molar volumes. Type H3 behavior is typical for CO_2-rich compositions, but the transition to type H2 and H4 can be only tentatively given due to the optical restriction to observe small amounts of liquid along the inclusion rim present at low temperatures. Type H4 is very common for CO_2–N_2 inclusions and characterized by partial homogenization (SLG → SL or SLG → SG) at temperatures below −147°C.

Of the S-type fluid inclusions, the type S2 behavior is by far most common. Type S2 (showing SLG → SL → L) is particularly important for N_2-rich fluids of low molar volume. The limits of the S2-field are defined by the conditions where melting and homogenization temperatures become equal ($T_h = T_m$). Type S1 (showing only SL → L) is rarely observed and found for extremely high densities (low molar volumes); types S3 and S4 have been ob-

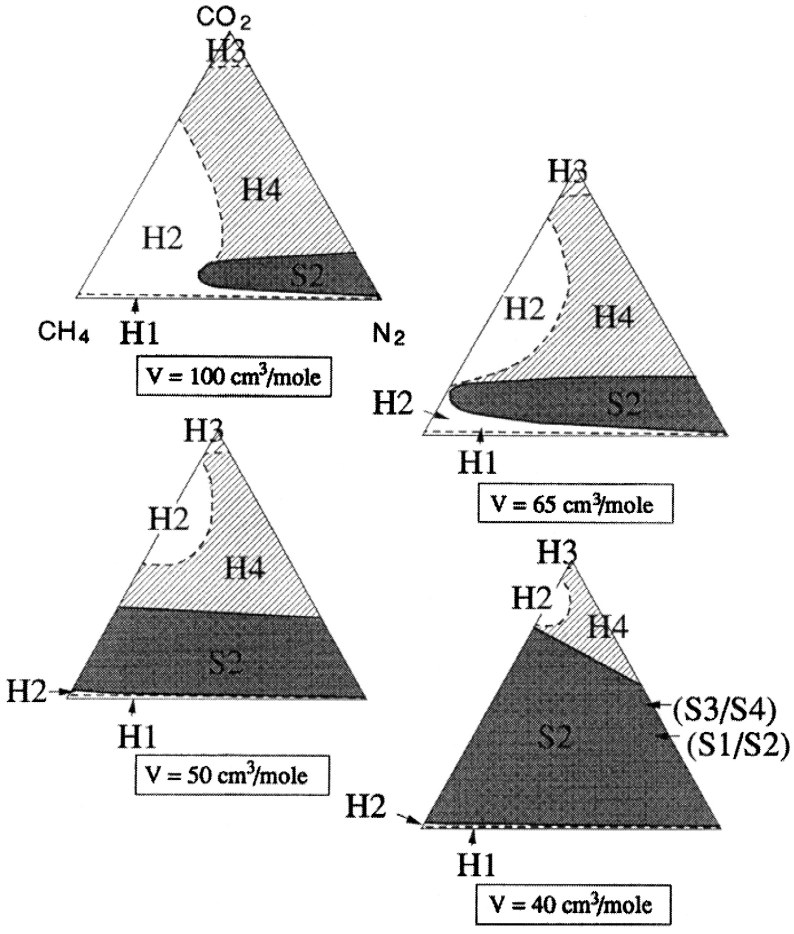

Fig. 13. Isochoric projections of the system CO_2–CH_4–N_2 showing the behavior on microthermometry runs in relation to composition and molar volume. Diagrams are shown for 40, 50, 65 and 100 cm^3/mole. Note that $T_h < T_m$ for the dark gray areas denoted by S2.

served for molar volumes < 40 cm^3/mole (Van den Kerkhof, 1988), type S3 also for the 'superdense' pure CO_2 inclusions (< 37.347 cm^3/mole) described earlier in this paper (Van den Kerkhof and Olsen, 1990; Frezzotti et al., 1992).

9. Conclusion

Phase diagrams, which graphically present the composition, molar volume and the temperature of a system without direct indication of the pressure (and therefore exotics in physics and chemistry) are highly useful and uniquely developed for the study of fluid inclusions. During the last decades, the parallel development of technical equipment for the microanalysis of fluid inclusions, i.e. improved heating/freezing stages and spectrometers, together with the progress made in the theoretical knowledge of phase transitions for most important fluid systems resulted in a highly practicable concept to determine the fluid *VX* properties. In our experience, microthermometry data interpreted with the actual phase diagrams show good agreement with results obtained by Raman analysis. However, there may be a difference in accuracy like the fact that the melting point depression for the system CO_2–N_2 is so small that compositions measured by Raman are always more accurate than those obtained from microthermometry alone. The limitation of the method mainly depends

on the reachable accuracy of calibrating heating/freezing stages and by possible extra admixtures like H_2S, higher hydrocarbons etc., compounds, which may highly complicate the phase behavior. However, in spite of attempts to measure independently the density (and internal pressure) in fluid inclusions (like from the peak properties of the Raman spectrum), microthermometry combined with phase diagrams remains the basic method to determine fluid inclusion densities.

References

Andersen, T., Austrheim, H., Burke, E.A.J., 1990. Fluid inclusions in granulites and eclogites from the Bergen Arcs, Caledonian of W. Norway. Mineral. Mag. 54, 145–158.

Andersen, T., Neumann, E.-R., 2001. Fluid inclusions in mantle xenoliths. Lithos 55, 299–318, (this volume).

Angus, S., Armstrong, B., de Reuk, K.M., 1976a. International thermodynamic tables of the fluid state, Methane vol. 5 Pergamon, Oxford.

Angus, S., Armstrong, B., de Reuk, K.M., 1979. International thermodynamic tables of the fluid state, Nitrogen vol. 6 Pergamon, Oxford.

Angus, S., Armstrong, B., de Reuk, K.M., Altunin, V.V., Gadetskii, O.G., Chapela, G.A., Rowlinson, J.S., 1976b. International thermodynamic tables of the fluid state, Carbon Dioxide vol. 3 Pergamon, Oxford.

Antanovish, A.A., Plotnikov, M.A., 1976. Experimental determination of the density of nitrogen at high pressures and temperatures. Sov. Phys. Dokl. 21, 99–100.

Arai, Y., Kaminishi, G., Saito, S., 1971. The experimental determination of the $P-V-T-X$ relations for the carbon dioxide–nitrogen and carbon dioxide–methane systems. J. Chem. Eng. Jpn. 4, 113–122.

Bakker, R.J., Jansen, J.B.H., 1993. Calculated fluid evolution path versus fluid inclusion data in the COHN system as exemplified by metamorphic rocks from Rogaland, south-west Norway. J. Metamorph. Geol. 11, 357–370.

Berdnikov, N.V., 1987. Thermobarogeochemistry: precambrian metamorphic complexes of the Far East (Russia). PhD Dissertation, Institute of Tectonics and Geophysics Far East Branch (Khabarovsk). Akad. NAUKA SSSR, Moscow, 115 pp.

Bottinga, Y., Richet, P., 1981. High pressure and temperature equation of state and calculation of the thermodynamic properties of gaseous carbon dioxide. Am. J. Sci. 281, 615–660.

Brown, P.E., 1989. FLINCOR: a microcomputer program for the reduction and investigation of fluid-inclusion data. Am. Mineral. 74, 1392–1395.

Burruss, R.C., 1981. Analysis of fluid inclusions: phase equilibria at constant volume. Am. J. Sci. 281, 1104–1126.

Darimont, A., Heyen, G., 1988. Simulation des équilibres de phases dans le système CO_2-N_2: applications aux inclusions fluides. Bull. Mineral. 111, 179–182.

Diamond, L., 1996. Isochoric paths in immiscible fluids and the interpretation of multicomponent fluid inclusions. Geochim. Cosmochim. Acta 60, 3825–3834.

Dubessy, J., Ramboz, C., 1986. The history of organic nitrogen from early diagenesis to amphibolite facies: mineralogical, chemical, mechanical and isotopic implications. 5th Internat. Symposium on Water–rock interaction. Reykjavik Extended Abstracts. pp. 170–174.

Frezzotti, M.L., Burke, E.A.J., De Vivo, B., Stefanini, B., Villa, I.M., 1992. Mantle fluids in pyroxenite nodules from Salt Lake Crater (Oahu, Hawaii). Eur. J. Mineral. 4, 1137–1153.

Guilhaumou, N., Dhamelincourt, P., Touray, J.C., Touret, J., 1981. Étude des inclusions fluides du système N_2-CO_2 de dolomites et de quartz de Tunisie septentrionale. Données de la microcryoscopie et de l'analyse à la microsonde à effet Raman. Geochim. Cosmochim. Acta 45, 657–673.

Herskowitz, M., Kisch, H.J., 1984. An algorithm for finding composition, molar volume and isochores of CO_2-CH_4 fluid inclusions from Th and Tfm (for Th < Tfm). Geochim. Cosmochim. Acta 48, 1581–1587.

Heyen, G., Ramboz, C., Dubessy, J., 1982. Simulation des équilibres de phases dans le système CO_2-CH_4 en dessous de 50°C et de 100 bar. Applications aux inclusions fluides. C.R. Acad. Sci. Paris, Ser. II t.294, 203–206.

Hoefs, J., Touret, J.L.R., 1975. Fluid inclusion and carbon isotope study from Bamble granulites (south Norway). Contrib. Mineral. Petrol. 52, 165–174.

Holloway, J.R., 1977. Fugacities and activity of molecular species in supercritical fluids. In: Fraser, D.G. (Ed.), Thermodynamics in Geology. NATO ASI, Series D Reidel, Dordrecht, pp. 161–181.

Huizenga, J.M., 1995. Fluid evolution in shear zones from the Late Archean Harare–Shamva–Bindura Greenstone Belt (NE Zimbabwe). PhD Dissertation, Free University, Amsterdam, 146 pp.

Huizenga, J.M., 2001. Thermodynamic modelling of C–O–H fluids. Lithos 55, 101–114, (this volume).

Juza, J., Kmonicek, V., Sifner, O., 1965. Measurements of the specific volume of carbon dioxide in the range of 700 to 4000 bar and 50 to 475°C. Physica 31, 1735–1744.

Kerrick, D.M., Jacobs, G.K., 1981. A modified Redlich–Kwong equation for H_2O, CO_2 and H_2O-CO_2 mixtures at elevated pressures and temperatures. Am. J. Sci. 281, 735–767.

Klemd, R., Van den Kerkhof, A.M., Horn, E.E., 1992. High-density CO_2-N_2 inclusions in eclogite-facies metasediments of the Münchberg Gneiss Complex, SE Germany. Contrib. Mineral. Petrol. 111, 409–419.

Kooi, M.E., Schouten, J.A., Van den Kerkhof, A.M., Istrate, G., Althaus, E., 1998. The system CO_2-N_2 at high pressure and applications to fluid inclusions. Geochim. Cosmochim. Acta 62, 2837–2843.

Kreglewski, A., Hall, K.R., 1983. Phase equilibria calculated for the systems N_2+CO_2, CH_4+CO_2 and CH_4+H_2S. Fluid Phase Equilib. 15, 11–32.

Kreulen, R., Schuiling, R.D., 1982. $N_2-CH_4-CO_2$ fluids during formation of the Dôme de l'Agout, France. Geochim. Cosmochim. Acta 46, 193–203.

Malbrunot, P., Vodar, B., 1973. Experimental PVT data and thermodynamic properties of nitrogen up to 1000°C and 5000 bar. Physica 66, 351–363.

Mullis, J., 1979. The system methane–water as a geological thermometer and barometer from the external part of the central Alps. Bull. Mineral. 102, 526–536.

Roedder, E., 1984. Fluid Inclusions. In: Ribbe, P.H. (Ed.), Reviews in Mineralogy vol. 12 Mineral. Soc. America, 644 pp.

Shmonov, V.M., Shmulovish, K.I., 1974. Molal volumes and equations of state of CO_2 at temperatures from 100 to 1000°C and pressures from 2000 to 10,000 bar. Dokl. Akad. Nauk SSSR 217 (4), 935–938.

Swanenberg, H.E.C., 1980. Fluid inclusions in high-grade metamorphic rocks from S.W. Norway. PhD Dissertation, University of Utrecht, Geologica Ultraiectina 25, 147 pp.

Thiéry, R., Van den Kerkhof, A.M., Dubessy, J., 1994b. vX properties of CH_4-CO_2 and CO_2-N_2 fluid inclusions: modelling for $T < 31$°C and $P < 400$ bars. Eur. J. Mineral. 6, 753–771.

Thiéry, R., Vidal, J., Dubessy, J., 1994a. Phase equilibria modelling applied to fluid inclusions. Liquid–vapour equilibria and calculation of the molar volume in the $CO_2-CH_4-N_2$ system. Geochim. Cosmochim. Acta 58, 1073–1082.

Touret, J.L.R., 1977. The significance of fluid inclusions in metamorphic rocks. In: Fraser, D.G. (Ed.), Thermodynamics in Geology. NATO ASI, Series D Reidel, Dordrecht, pp. 203–227.

Touret, J.L.R., 1992. CO_2 transfer between the upper mantle and the atmosphere: temporary storage in the lower continental crust. Terra Nova 4, 87–98.

Tsiklis, D.S., Polyakov, E.V., 1968. Measuring the compressibility of gases by displacement method. Nitrogen compressibility at pressures up to 10,000 atm. and temperatures to 400°C. Dokl. Akad. Nauk., Sov. Phys. 12 (9), 901–904.

Vagarftik, N.B., 1972. Tables of thermodynamic properties of gases and liquids. Izd. Nauka, Moscow, 720 pp.

Van den Kerkhof, A.M., 1988. The system $CO_2-CH_4-N_2$ in fluid inclusions: theoretical modelling and geological applications. PhD Dissertation, Amsterdam (Free University), 206 pp.

Van den Kerkhof, A.M., 1990. Isochoric phase diagrams in the systems CO_2-CH_4 and CO_2-N_2: applications to fluid inclusions. Geochim. Cosmochim. Acta 54, 621–629.

Van den Kerkhof, A.M., Frezzotti, M.L., Talarico, F., Berdnikov, N.V., 1993. Metastable phase transitions in the system $CO_2-CH_4-N_2$ including immiscibility of the undercooled liquid (L1L2G): an example from granulites of the Wilson terrane, North Victoria Land (Antarctica). ECROFI XII Abstract (Warsaw). Archiwum Mineralogische vol. XLIX pp. 227–229.

Van den Kerkhof, A.M., Kreulen, R., Touret, J.L.R., 1994. Juvenile CO_2 in enderbites of Tromøy near Arendal, southern Norway: a fluid inclusion and stable isotope study. J. Metamorph. Geol. 12, 301–310.

Van den Kerkhof, A.M., Olsen, S.N., 1990. A natural example of superdense CO_2 inclusions: microthermometry and Raman analysis. Geochim. Cosmochim. Acta 54, 895–901.

Van den Kerkhof, A.M., Touret, J.L.R., Mayer, C., Jansen, J.B.H., 1991. Retrograde methane-dominated fluid inclusions from high-temperature granulites of Rogaland, southwestern Norway. Geochim. Cosmochim. Acta 55, 2533–2544.

Van Konynenburg, P.H., Scott, R.L., 1980. Critical lines and phase equilibria in binary Van der Waals mixtures. Philos. Trans. R. Soc., Ser. A 298, 495–540.